

Supporting Information

Integrated Selective Nitrite Reduction to Ammonia with Tetrahydroisoquinolines Semi-dehydrogenation over a Vacancy-Rich Ni Bifunctional Electrode

Changhong Wang,^{#a} Wei Zhou,^{#b} Zhaojun Sun,^b Yuting Wang,^b Bin Zhang^{a,b} and Yifu Yu^{*a}

^aInstitute of Molecular Plus, Tianjin University, Tianjin 300072, China.

^bSchool of Science, Key Laboratory of Molecular Optoelectronic Sciences, Tianjin University, Tianjin 300072, China.

[#]These authors contributed equally to this work.

*E-mail: yfu@tju.edu.cn

1. Experimental Procedures

1.1 Materials Preparation.

1.1.1 Fabrication of Ni(OH)₂ nanosheet arrays supported on nickel foam.

Firstly, nickel foam (1×3 cm²) is sonicated with acetone, 1 M HCl aqueous solution and deionized water for 15 min, respectively. After 2 mmol Ni(NO₃)₂·6H₂O and 4 mmol Hexamethylenetetramine dissolved in 15 mL deionized water in a 20 mL Teflon-lined stainless-steel autoclave, one piece of freshly-treated nickel foam is added. The autoclave is sealed and treated at 100 °C for 10 h and then cooled down to room temperature naturally. The green Ni(OH)₂ nanosheet arrays supported on nickel foam is obtained after rinsing with deionized water and drying in a vacuum oven.

1.1.2 Fabrication of Ni nanosheet arrays supported on nickel foam (Ni-NSA).

In a typical procedure, 0.5 g NaOH and 15 ml Ethylene Glycol are put into a 20 mL Teflon-lined stainless-steel autoclave. Then, Ni(OH)₂ nanosheet arrays supported on nickel foam are added to the Teflon-lined stainless-steel autoclave and maintained at 160 °C for 12 h, and then cooled down to room temperature naturally. The Ni-NSA is obtained after rinsing with deionized water and drying in a vacuum oven. The as-obtained Ni-NSA should be stored in the environment without oxygen to avoid oxidation.

1.1.3 Synthesis of Ni nanosheet arrays with nickel vacancies supported on nickel foam (Ni-NSA-V_{Ni}).

A piece of Ni-NSA is put on the bottom of the quartz boat and treated by plasma (commercial 13.56 MHz RF source) in the H₂/Ar (3 vol% H₂) atmosphere for 5 min with the power of 200W, the pressure of 90 Pa and gas flow rate of 100 mL min⁻¹. The as-obtained Ni-NSA-V_{Ni} should be stored in the environment without oxygen to avoid oxidation.

1.1.4 Synthesis of Ni nanosheet arrays with nickel vacancies supported on copper foam (Ni-NSA-V_{Ni}/Cu Foam) for the XRD test.

The procedure for the fabrication of Ni-NSA-V_{Ni}/Cu Foam is the same as that of Ni-NSA-V_{Ni}, except that the nickel foam is replaced by copper foam.

1.2 Materials Characterizations.

The scanning electron microscope (SEM) images are obtained by Hitachi S-4800. Transmission electron microscopy (TEM) and high-resolution transmission electron microscopy (HRTEM) images are taken on the

JEOL-2100F system. Powder X-ray diffraction (XRD) data is acquired on a Bruker D8 Focus Diffraction System with a Cu K α radiation ($\lambda = 0.154178$ nm). X-ray photoelectron spectroscopy (XPS) measurements are performed with a Perkin Elmer PHI 1600 Versa Probe with Al K α as the excitation source. All binding energies are revised according to the C 1s peak at 284.8 eV. The X-ray absorption fine structure spectroscopy (XAFS) measurements are undertaken at Beamline 1W1B of the Beijing Synchrotron Radiation Facility (BSRF). The XAFS data are recorded under transmission mode and the energy calibration was adopted using standard Ni foam. Demeter package is used to extract the data and fit the profiles for data processing. The thickness of nanosheets is determined by atomic force microscopy (AFM) (Bruker multimode 8). UV-Vis absorbance spectra are measured on a Beijing Purkinje General T6 new century spectrophotometer. The differential electrochemical mass spectrometry (DEMS, QAS 100) is provided by Linglu instruments (Shanghai) Co. Ltd to perform *in situ* analysis of produced intermediates and products. The isotope labeling experiments are measured by ^1H -NMR measurement (Bruker 600-MHz system). Raman spectroscopy is tested on inVia reflex Raman microscope under an excitation of 532 nm laser light. For *in situ* Raman test, the cell is homemade by Teflon with a quartz window between the sample and objective. The working electrode is immersed into the electrolyte through the wall of the cell and keeps the electrode plane perpendicular to the laser. A platinum wire and saturated calomel electrode are served as the counter and reference electrode, respectively.

1.3 Electrochemical Measurements.

1.3.1 Electrochemical measurements of nitrite reduction.

The electrochemical measurements are conducted using a CHI 660D electrochemical workstation (Chenhua, Shanghai). A typical H-type electrolytic cell separated by AlkymerTM alkaline membrane (AE-125) is used. All electrochemical tests are performed in a standard three-electrode electrochemical cell with the as-prepared samples on Ni foam (1×1 cm²) as the working electrode, Pt plate (1×1 cm²) as the counter electrode and saturated calomel electrode (SCE) used as reference electrode at room temperature. In all measurements, the data is *iR* corrected. All the polarization curves are the steady-state ones after several cycles with a scan rate of 5 mV s⁻¹, and current density is normalized to the geometric surface area. 0.2 M Na₂SO₄ solution (60 mL) is used as an electrolyte and evenly distributed to the cathode and anode compartment. NaNO₂ (200 mg L⁻¹) is added into the cathode compartment as the reactant. Prior to NO₂⁻ electroreduction test, cathode electrolyte is purged with Ar (99.99 % purity) for 30 min. The potentiostatic test is conducted at different potentials for 2 h at a stirring rate of ~500 rpm.

1.3.2 Electrochemical measurements for semi-dehydrogenation of tetrahydroisoquinolines (THIQs).

Electrochemical measurements for semi-dehydrogenation of THIQs are carried out in a standard three-compartment electrochemical cell consisting of a working electrode, a Pt counter electrode, and an Ag/AgCl (1.0 M KCl) reference electrode. Linear sweep voltammetry (LSV) without iR compensation is performed using an electrochemical workstation (CHI 660E, Chenhua, Shanghai). The solution of 1.0 M KOH (pH=13.6), which is purified according to the previous method,¹ is employed as the electrolyte. All potentials measured are calibrated to a reversible hydrogen electrode (RHE) using the Eq. S1:

$$E_{\text{RHE}} = E_{\text{Ag/AgCl}} + 0.197 + 0.0591 \times \text{pH} \quad (\text{Eq. S1})$$

The nickel foam with catalyst samples directly grown on the surface is used as the working electrode with an exposed surface area of 1.0 cm². The electrochemical OER and semi-dehydrogenation of THIQs experiments over Ni-NSA-V_{Ni} anode are conducted in 25 mL of 1.0 M KOH solution with and without 0.5 mmol THIQs.

1.3.3 Electrochemical measurements for electrocatalytic semi-dehydrogenation of THIQs coupled with electroreduction of nitrite to ammonia over bifunctional electrodes.

For two-electrode electrolysis, Ni-NSA-V_{Ni} electrode is employed as both anode and cathode. The scan rate of LSV curves is 5 mV s⁻¹ with 1.0 M KOH as the electrolyte for electrocatalytic semi-dehydrogenation of THIQs and 0.2 M Na₂SO₄ electrolyte for nitrite reduction. All experiments are carried out at room temperature. *In situ* Raman spectra is recorded on the aforementioned confocal Raman microscope under chronoamperometry test at 1.4 V versus RHE in 0.1 M KOH solution by the electrochemical workstation. The electrolytic cell is homemade by Teflon with a thin round quartz glass plate as cover to protect the objective. The self-supported working electrodes are inserted through the wall of the cell to keep the plane of the working electrode perpendicular to the incident laser. Prior to the measurements, the working electrodes are carefully covered with epoxy and Teflon tape to ensuring an exposed area of 0.25 cm².

1.4 Ion concentration detection methods.

The electrolytes pre- and post-test are firstly diluted to an appropriate concentration and then tested by UV-Vis spectrophotometer to quantify the concentration. The concentrations of nitrite-N and ammonia-N are estimated by UV-Vis spectrophotometry according to the standard method. The specific approaches are as follows.

1.4.1 Determination of nitrite-N.

A mixture of *p*-aminobenzenesulfonamide (4 g), *N*-(1-Naphthyl) ethylenediamine dihydrochloride (0.2 g), ultrapure water (50 mL) and phosphoric acid (10 mL, $\rho = 1.70$ g/mL) is used as a color reagent. A certain amount of electrolyte is taken from the electrolytic cell and diluted to 5 mL to the detection range. Next, 0.1 mL color reagent is added into the aforementioned 5 mL solution and mixed to uniformity, and the absorption intensity at a wavelength of 540 nm is recorded after sitting for 20 min. The concentration–absorbance curve is calibrated using a series of standard sodium nitrite solutions.

1.4.2 Determination of ammonia-N.

Ammonia-N is determined using Nessler's reagent as the color reagent. First, a certain amount of electrolyte is taken from the electrolytic cell and diluted to 5 mL to the detection range. Next, 0.1 mL potassium sodium tartrate solution ($\rho = 500$ g/L) is added and mixed thoroughly, then 0.1 mL Nessler's reagent is put into the solution. The absorption intensity at a wavelength of 420 nm is recorded after sitting for 20 min. The concentration–absorbance curve is made using a series of standard ammonium chloride solutions and the ammonium chloride crystal is dried at 105 °C for 2 h in advance.

1.5 ^{15}N Isotope Labeling Experiments.

99.24% $\text{Na}^{15}\text{NO}_2$ is used as the feeding N-source to perform the isotopic labeling nitrite reduction experiments. 0.2 M Na_2SO_4 is used as electrolyte and $\text{Na}^{15}\text{NO}_2$ with a concentration of 200 ppm $^{15}\text{NO}_2\text{-N}$ is added into the cathode compartment as the reactant. After electroreduction for 2 h at -1.2 V vs. SCE, 20 ml post-tested electrolyte with obtained $^{15}\text{NH}_4^+$ is took out and the pH value is adjusted to be weak acid with 4 M H_2SO_4 . Then the solution is volumed to 25 ml in the volumetric flask with 0.2 M Na_2SO_4 for further quantification by ^1H NMR (600 MHz) with external standards, which take maleic acid ($\text{C}_4\text{H}_4\text{O}_4$, 125 ppm) as a reference. The calibration curve is created as follows: First, a series of $^{15}\text{NH}_4^+$ solutions ($(^{15}\text{NH}_4)_2\text{SO}_4$) with known concentration are prepared in 0.2 M Na_2SO_4 as standards; Second, 50 mL of the $^{15}\text{NH}_4^+$ standard solution with different concentration is mixed with maleic acid (125 ppm); Third, 50 μL deuterium oxide (D_2O) is added in 0.5 mL above mixed solution for the NMR detection; Fourth, the calibration is achieved using the peak area ratio between $^{15}\text{NH}_4^+$ and maleic acid because the $^{15}\text{NH}_4^+$ concentration and the area ratio are positively correlated. Similarly, the amount of $^{14}\text{NH}_4^+$ is quantified by this method when $\text{Na}^{14}\text{NO}_2$ is used as the feeding N-source.

1.6 Calculation of the selectivity, conversion, Faradaic efficiency and yield.

For the NO_2^- electroreduction experiments, the selectivity of NH_3 is acquired by Eq. S2:

$$\text{Selectivity} = c_{\text{NH}_3} / \Delta c_{\text{NO}_2^-} \times 100\% \quad (\text{Eq. S2})$$

The conversion of NO_2^- is obtained from Eq. S3:

$$\text{Conversion} = \Delta c_{\text{NO}_2^-} / c_0 \times 100\% \quad (\text{Eq. S3})$$

where c_{NH_3} is the concentration of $\text{NH}_3(\text{aq})$, $\Delta c_{\text{NO}_2^-}$ is the concentration difference of NO_2^- before and after electrolysis, c_0 is the initial concentration of NO_2^- .

The Faradaic efficiency is estimated from the charge consumed for NO_2^- reduction and total charge pass through the electrode by using Eq. S4:

$$\text{Faradaic efficiency} = (6F \times c_{\text{NH}_3} \times V) / (M_{\text{NH}_3} \times Q) \quad (\text{Eq. S4})$$

(Note that the reduction of NO_2^- to NH_3 consume six electrons.)

where F is the Faradaic constant (96485 C mol^{-1}), c_{NH_3} is the concentration of NH_3 , V is the volume of electrolyte in the anode compartment, M_{NH_3} is the molar mass of NH_3 , Q is the total charge passing the electrode.

The yield of $\text{NH}_3(\text{aq})$ is calculated using Eq. S5:

$$\text{Yield}_{\text{NH}_3} = (c_{\text{NH}_3} \times V) / (M_{\text{NH}_3} \times t \times S) \quad (\text{Eq. S5})$$

where c_{NH_3} is the concentration of NH_3 , V is the volume of electrolyte in the anode compartment, M_{NH_3} is the molar mass of NH_3 , t is the electrolysis time, S is the electrochemical active surface area (ECSA) of catalysts determined by electrochemical capacitance measurements.

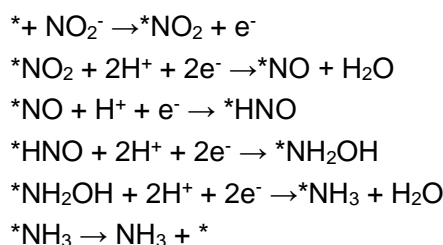
For the electrocatalytic semi-dehydrogenation of THIQs experiments, the selectivity (%) of DHIQs formation were calculated using Eq. S6:

$$\text{Selectivity (\%)} = \frac{\text{mol of formed DHIQs}}{\text{mol of consumed THIQs}} \times 100\% \quad (\text{Eq. S6})$$

1.7 Theoretical calculation details.

In this work, all calculations are performed using the Vienna ab initio simulation package (VASP) based on the density functional theory (DFT).^{2,3} The projected augmented wave (PAW) method with PBE functional is chosen here.⁴ The kinetic energy cutoff for the plane-wave expansion is set to 400 eV. The 3×3×1 k-point mesh set is used for the slab models of Ni (111) plane with five atomic layers. And a vacuum layer of 16 Å is introduced to avoid the interaction between neighboring slab modes along the out-plane direction. All the structural models are fully relaxed to the ground state with the convergence of energy and forces setting to 10⁻⁵ eV and 0.01 eV/Å, respectively. In addition, the DFT-D2 method of Grimme is used to describe the long-range dispersion interaction.⁵

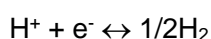
To calculate the reaction free energy, the chemical reaction equations are summarized below:



where * represents the slab model with the active site. Then, the reaction free energy change can be obtained with Eq. S7:

$$\Delta G = \Delta E + \Delta E_{\text{ZPE}} - T\Delta S \quad (\text{Eq. S7})$$

where ΔE is the total energy difference between the products and the reactants of each reaction step, ΔE_{ZPE} and ΔS are the differences of zero-point energy and entropy, respectively. The zero-point energy of free molecules and adsorbates were obtained from the vibrational frequency calculations. The free energy change of each step that involves an electrochemical proton-electron transfer was described by the computational hydrogen electrode (CHE) model proposed by Nørskov et al.⁶ In this technique, zero voltage is defined based on the reversible hydrogen electrode (RHE), in which the reaction is defined to be in equilibrium at zero voltage, at all values of pH, at all temperatures, and with H₂ at 101325 Pa pressure.



Therefore, in the CHE model, the free energy of a proton-electron pair, $G_{(\text{H}^+ + \text{e}^-)}$ is equal to half of the free energy of gaseous hydrogen ($1/2 G_{\text{H}_2}$) at a potential of 0 V.

To describe the charged NO₂⁻ species as a reference, the neutral HNO₂ gas phase was chosen as reference

and then the energy of nitrite ion was obtained from the thermodynamic cycle to avoid the difficulty of using periodic DFT calculations for charged systems.⁷

2. Result and Discussion

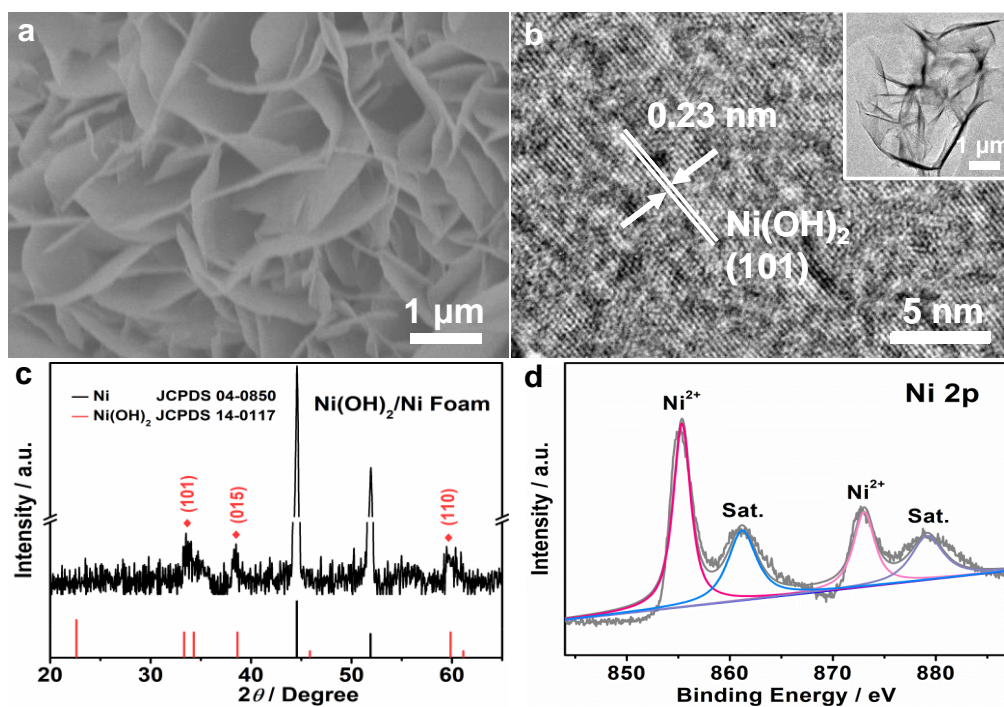


Figure S1. (a) SEM image, (b) HRTEM image, (inset in b) TEM image, (c) XRD pattern and (d) XPS spectra of Ni(OH)₂ nanosheet arrays supported on Ni foam. These results indicated that Ni(OH)₂ nanosheet arrays supported on Ni foam were successfully prepared.

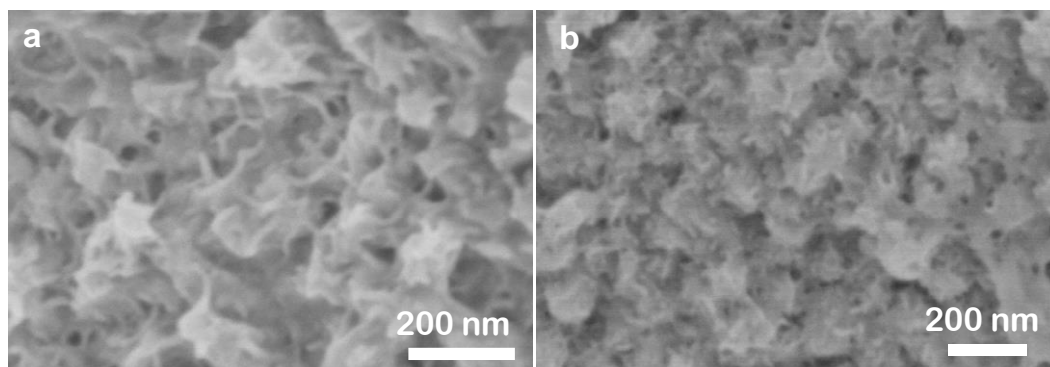


Figure S2. SEM images of (a) Ni-NSA and (b) Ni-NSA-V_{Ni}.

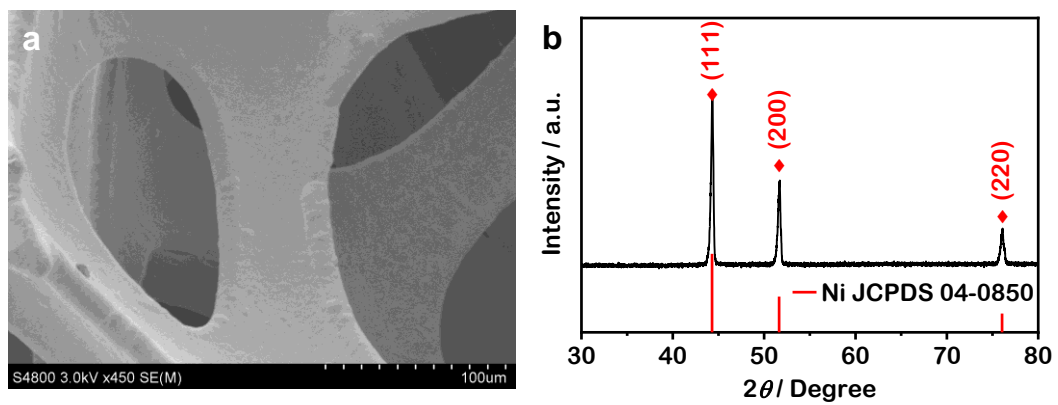


Figure S3. (a) SEM image and (b) XRD pattern of Ni Foam.

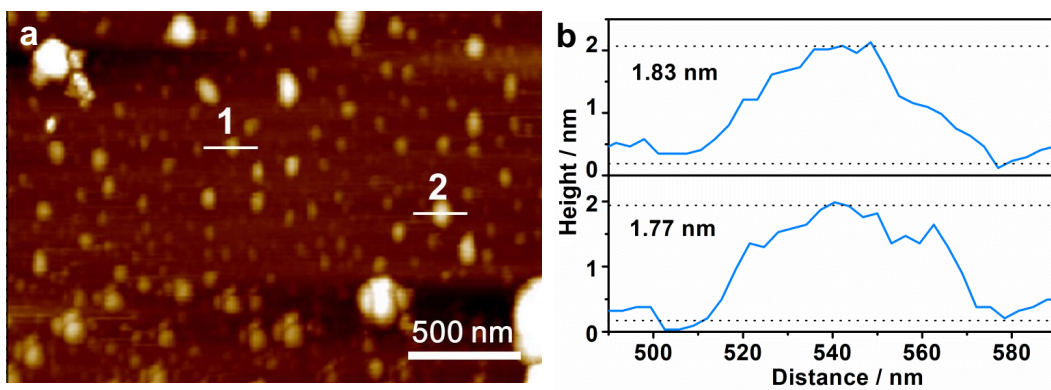


Figure S4. (a) AFM image of Ni-NSA- V_{Ni} . (b) The height profile of Ni-NSA- V_{Ni} after exfoliation from Ni foam.

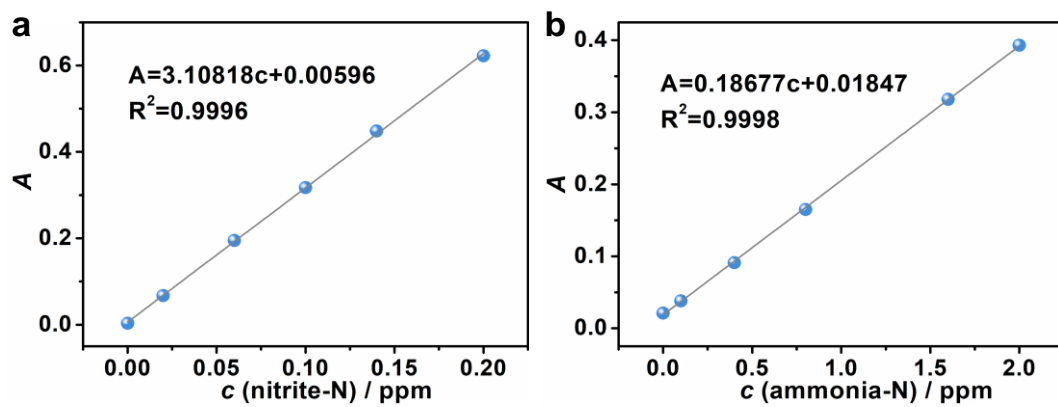


Figure S5. The UV-Vis absorption spectra and the corresponding calibration curves of (a) nitrite-N and (b) ammonia-N.

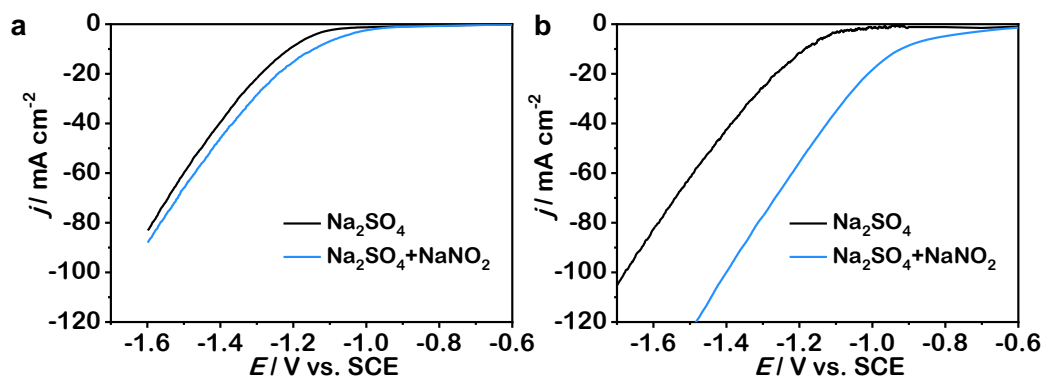


Figure S6. LSV curves of (a) Ni Foam and (b) Ni-NSA- V_{Ni} in 0.2 M Na_2SO_4 electrolyte with and without 200 mg L^{-1} NaNO_2 .

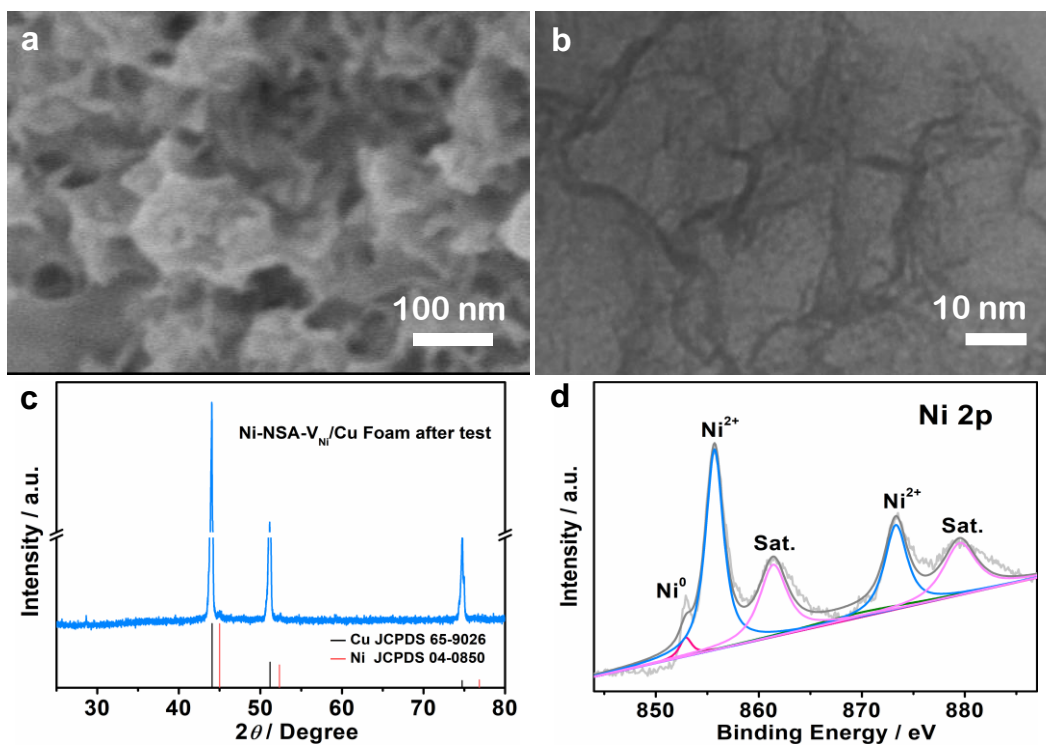


Figure S7. (a) Low-magnification SEM image, (b) TEM image, (c) XRD pattern and (d) XPS spectra of Ni-NSA- V_{Ni} after stability test.

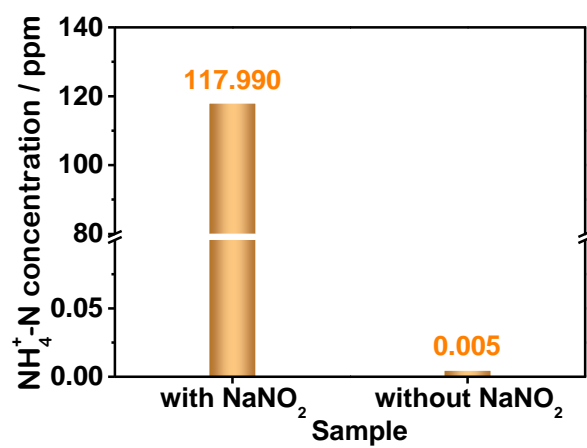


Figure S8. The concentration of $\text{NH}_4^+\text{-N}$ after electroreduction over Ni-NSA- V_{Ni} in 0.2 M Na_2SO_4 electrolyte with and without NO_2^- .

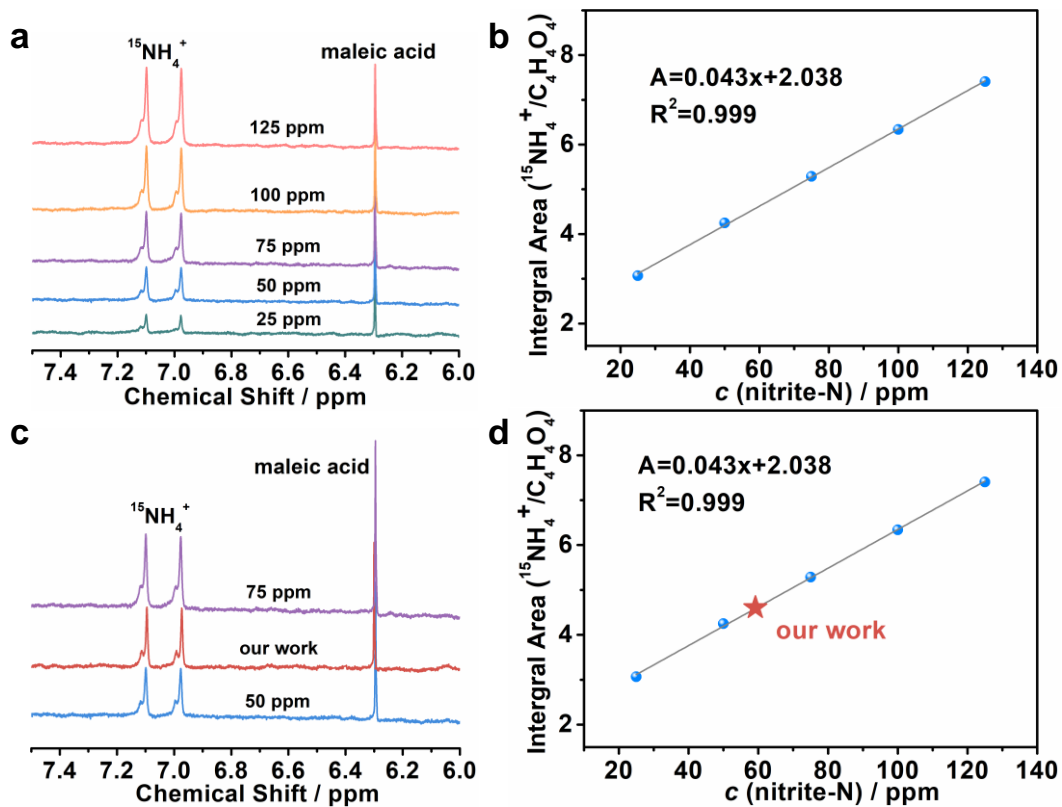


Figure S9. (a) ^1H NMR spectra (600 MHz) of various $^{15}\text{NH}_4^+$ ion concentration ($^{15}\text{NH}_4^+\text{-N}$) with maleic acid as the reference (125 ppm). (b) Integral area ($^{15}\text{NH}_4^+ / \text{C}_4\text{H}_4\text{O}_4$) against $^{15}\text{NH}_4^+$ ion concentration ($^{15}\text{NH}_4^+\text{-N}$). (c) ^1H NMR spectra (600 MHz) of the electrolyte after $^{15}\text{NO}_2^-$ reduction over Ni-NSA- V_{Ni} electrode at -1.2 V vs. SCE for 2 h. (d) The $^{15}\text{NH}_4^+$ ion concentration ($^{15}\text{NH}_4^+\text{-N}$) of the electrolyte was quantified by ^1H NMR with maleic acid (125 ppm) as the reference.

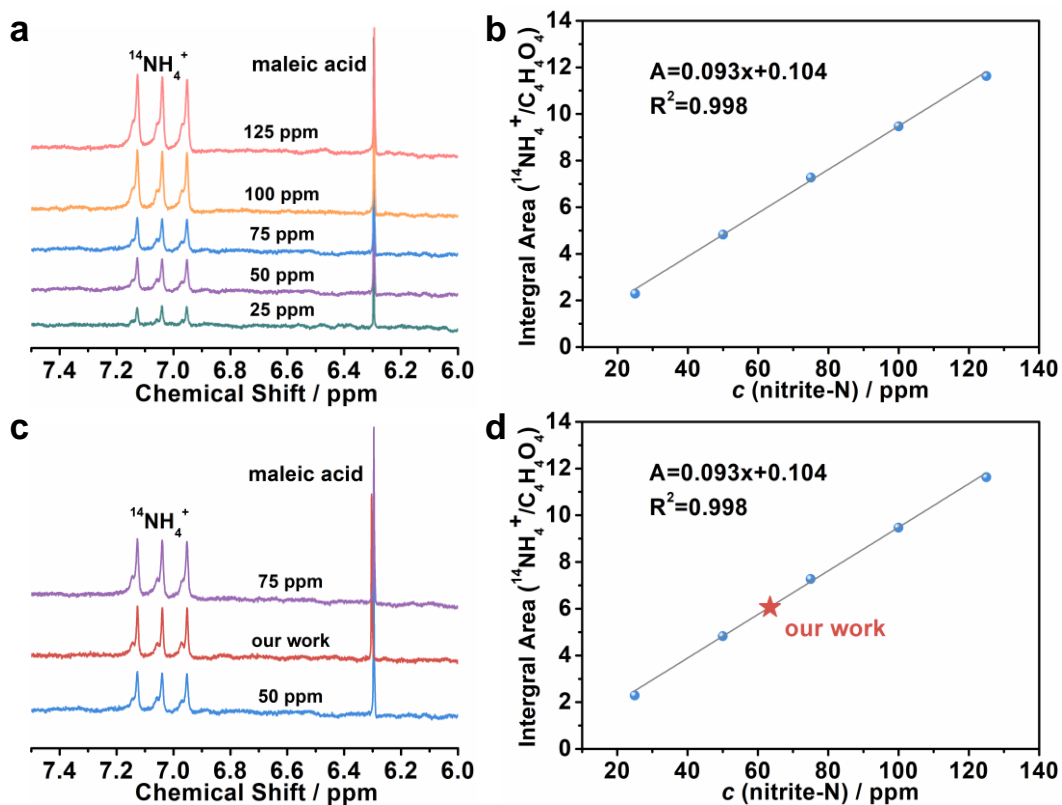


Figure S10. (a) ^1H NMR spectra (600 MHz) of various $^{14}\text{NH}_4^+$ ion concentration ($^{14}\text{NH}_4^+\text{-N}$) with maleic acid as the reference (125 ppm). (b) Integral area ($^{14}\text{NH}_4^+/\text{C}_4\text{H}_4\text{O}_4$) against $^{14}\text{NH}_4^+$ ion concentration ($^{14}\text{NH}_4^+\text{-N}$). (c) ^1H NMR spectra (600 MHz) of the electrolyte after $^{14}\text{NO}_2^-$ reduction over Ni-NSA- V_{Ni} electrode at -1.2 V vs. SCE for 2 h. (d) The $^{14}\text{NH}_4^+$ ion concentration ($^{14}\text{NH}_4^+\text{-N}$) of the electrolyte that was quantified by ^1H NMR with maleic acid (125 ppm) as the reference.

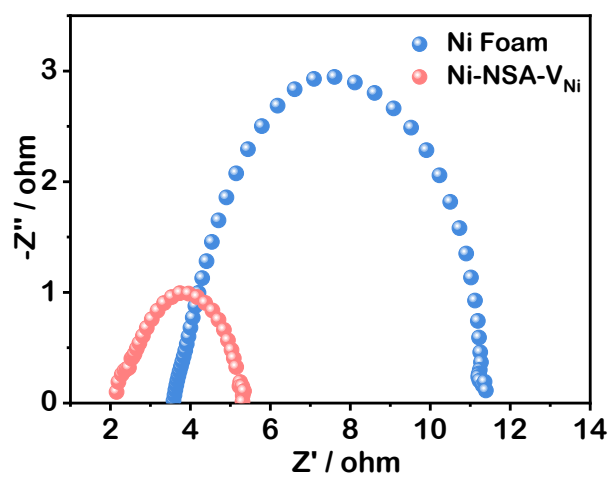


Figure S11. EIS spectra of Ni Foam and Ni-NSA-V_{Ni} at -1.2 V vs. SCE from 100 KHz to 1 Hz.

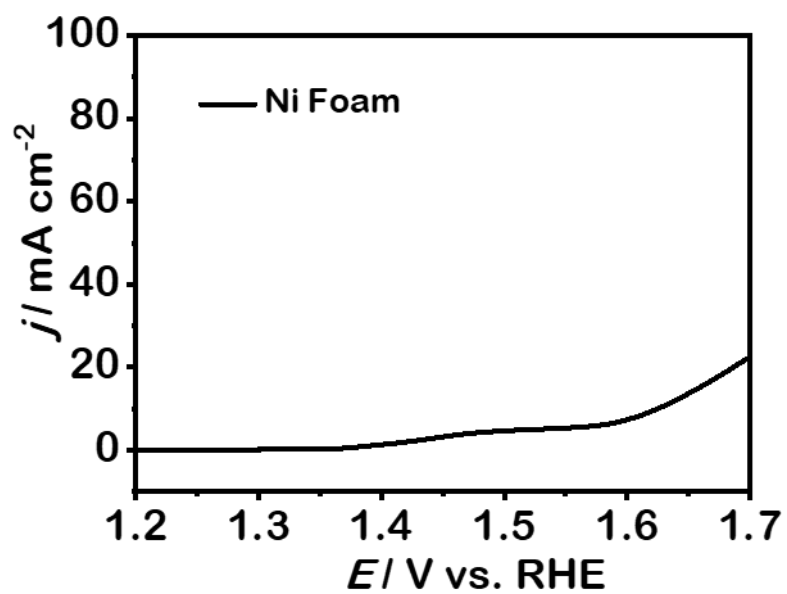


Figure S12. LSV curves of Ni Foam anode at a scan rate of 5 mV s^{-1} in 1.0 M KOH electrolyte with 0.5 mmol 1a .

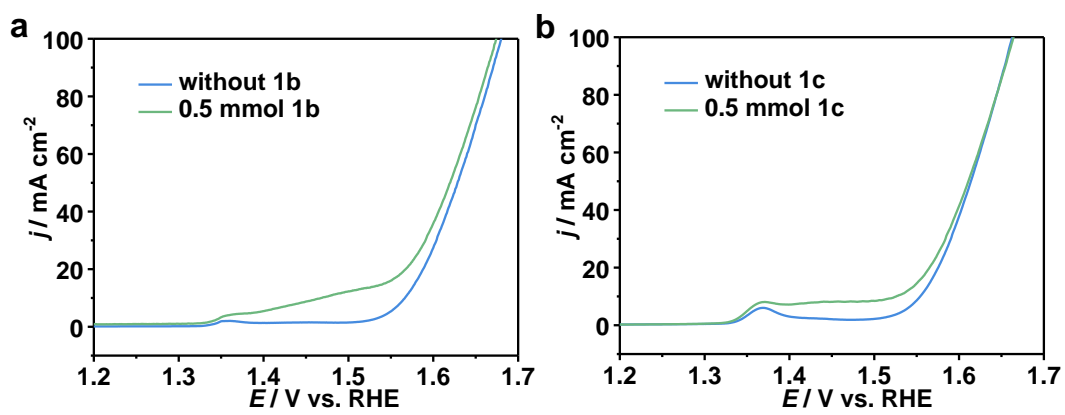


Figure S13. LSV curves of Ni-NSA- V_{Ni} for semi-dehydrogenation of (a) **1b** and (b) **1c** in 1.0 M KOH electrolyte.

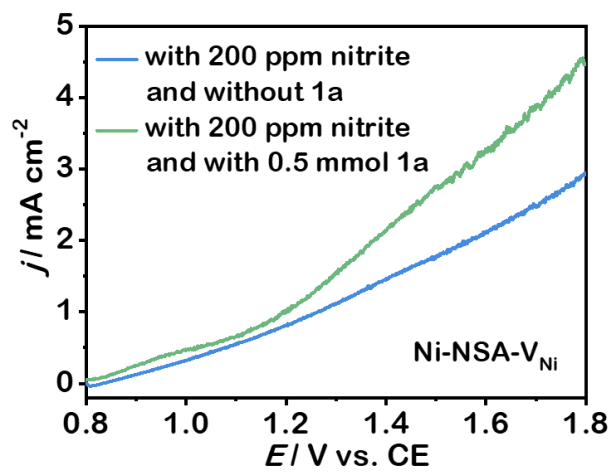


Figure S14. LSV curves in a Ni-NSA-V_{Ni} || Ni-NSA-V_{Ni} two-electrode cell.

Table S1 EXAFS Fitting Parameters of Ni Foam and Ni-NSA-V_{Ni}.

Sample	<i>N</i>	<i>R</i> (Å)
Ni foam	12	—
Ni-NSA-V _{Ni}	10.2	2.48

N is the coordination number. *R* is the distance between absorber and backscatter atom, determined by curve fitting. Error bounds (accuracies) characterizing the structural parameters obtained by EXAFS spectroscopy are estimated as follows: ± 0.2 for *N* and ± 0.01 Å for *R*.

Table S2 Comparison of the selective nitrite reduction activity of Ni-NSA- V_{Ni} with those of other catalysts for ammonia synthesis from nitrogen, nitrate and nitrite reduction.

Process	Catalyst	System	Condition	Performance	Testing method	Ref.
Electrocatalytic N_2 reduction	Fe_3Mo_3C/C	Pt 1 M KOH (-0.5 V vs. RHE)	25 °C 0.7 MPa	Y (NH_3): 13.55 $\mu g\ h^{-1}\ cm^{-2}$ (0.8 $\mu mol\ h^{-1}\ cm^{-2}$) FE (NH_3): 14.74%	Indophenol blue method 1H NMR	Ref. 8
	Phosphorus-doped carbon/Sb/SbPO ₄	Graphite 0.1 M Na ₂ SO ₄ (-0.15 V vs. RHE)	Ambient conditions	Y (NH_3): 25 $\mu g\ h^{-1}\ mg_{cat}^{-1}$ (0.29 $\mu mol\ h^{-1}\ cm^{-2}$) FE (NH_3): 31%	Indophenol blue method	Ref. 9
	Ru/MoS ₂	Pt wire 10 mM HCl (-0.15 V vs. RHE)	50 °C 0.1 MPa	Y (NH_3): 1.14 $\times 10^{-10}$ mol $cm^{-2}\ s^{-1}$ (0.41 $\mu mol\ h^{-1}\ cm^{-2}$) FE (NH_3): 14.6%	Indophenol blue method	Ref. 10
	Ru SAs/N-C	Graphite 0.05 M H ₂ SO ₄ (-0.2 V vs. RHE)	Ambient conditions	Y (NH_3): 120.9 $\mu g\ h^{-1}\ mg_{cat}^{-1}$ (0.45 $\mu mol\ h^{-1}\ cm^{-2}$) FE (NH_3): 29.6%	Indophenol blue method	Ref. 11
	B ₄ C nanosheet	Graphite 0.1 M HCl (-0.75 V vs. RHE)	Ambient conditions	Y (NH_3): 26.57 $\mu g\ h^{-1}\ mg_{cat}^{-1}$ (0.16 $\mu mol\ h^{-1}\ cm^{-2}$) FE (NH_3): 15.95%	Indophenol blue method	Ref. 12
	Bismuth nanocrystals	Pt plate K ₂ SO ₄ / H ₂ SO ₄ (-0.6 V vs. RHE)	Ambient conditions	Y (NH_3): 52 $\mu mol\ h^{-1}\ cm^{-2}$ FE (NH_3): 66%	Nessler's reagent Ammonia kit 1H NMR	Ref. 13
	Mo ⁰ /graphdiyne	Graphite 0.1 M Na ₂ SO ₄ (-1.2 V vs. SCE)	Ambient conditions	Y (NH_3): 145.4 $\mu g\ h^{-1}\ mg_{cat}^{-1}$ FE (NH_3): 21%	Indophenol blue method	Ref. 14
	Li ⁺ -incorporation poly(N-ethylbenzene -1,2,4,5-tetracarboxy lic diimide	Pt plate 0.5 M Li ₂ SO ₄ (-0.7 V vs. RHE)	Ambient conditions	0.12 $\mu mol\ h^{-1}\ cm^{-2}$ FE (NH_3): 2.85%	Nessler's reagent	Ref. 15

	Hemin-pyrolitic graphite electrode	Pt flag Phosphate buffer solutions (ionic strength 0.1 M), NaNO ₂ (acidic media)	Ambient conditions	S (NH ₂ OH): ~100%	Rotating Ring-Disk (RRDE) experiments and online electrochemical mass spectrometry	Ref. 23
	Ni-NSA-V _{Ni}	Pt plate 0.2 M Na ₂ SO ₄ , 200ppm NaNO ₂ -N (-1.2 V vs. Hg/Hg ₂ Cl ₂ , 2 h)	Ambient conditions	Y (NH ₃): 235.98 μmol h ⁻¹ cm ⁻² FE(NH ₃): 88.9% S (NH ₃): 77.2% R (NO ₂ ⁻): 73.4%	UV-vis spectroscopy and 1H NMR	our work

Note:

Y (NH₃): The yield of ammonia;

FE (NH₃): The Faradaic efficiency of ammonia;

S (NH₃): The selectivity of ammonia;

S (NO₂⁻): The selectivity of nitrite;

S (N₂): The selectivity of N₂;

R (NO₂⁻): The conversion rate of nitrite;

c(NH₃): The concentration of ammonia;

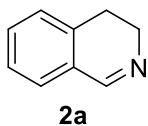
S (NH₂OH): The selectivity of NH₂OH.

Table S3. Comparison of the ammonia concentration obtained by electroreduction of nitrite over Ni-NSA-V_{Ni} using different quantitative methods.

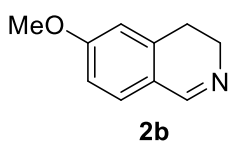
Electrode	Conditions	Quantitative method	NH ₄ ⁺ -N Concentration (ppm)
Ni-NSA-V _{Ni}	Na ¹⁴ NO ₂ , 25 °C -1.2 V vs. SCE (2 h)	Nessler's reagent	64.68
Ni-NSA-V _{Ni}	Na ¹⁴ NO ₂ , 25 °C -1.2 V vs. SCE (2 h)	1H NMR	63.66
Ni-NSA-V _{Ni}	Na ¹⁵ NO ₂ , 25 °C -1.2 V vs. SCE (2 h)	1H NMR	59.40

The calculated peak areas and corresponding ammonia yields of ¹⁵NH₄⁺ and ¹⁴NH₄⁺ by 1H NMR are very close to the quantitative results of colorimetric methods using Nessler's reagent.

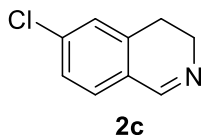
NMR and GC-MS data



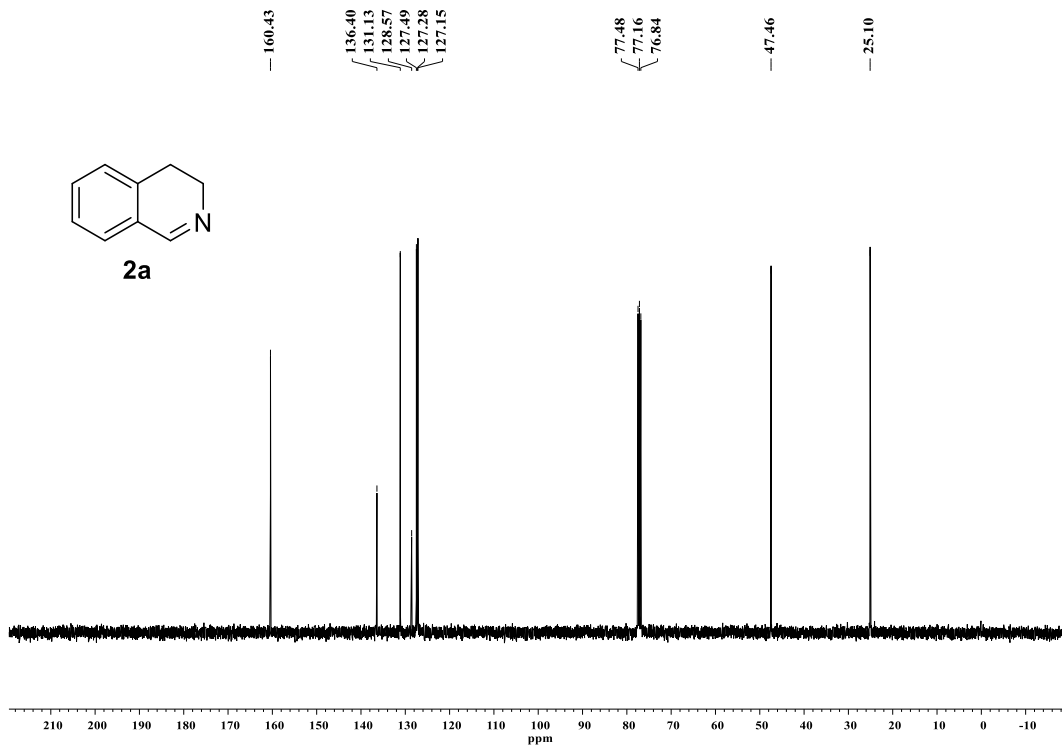
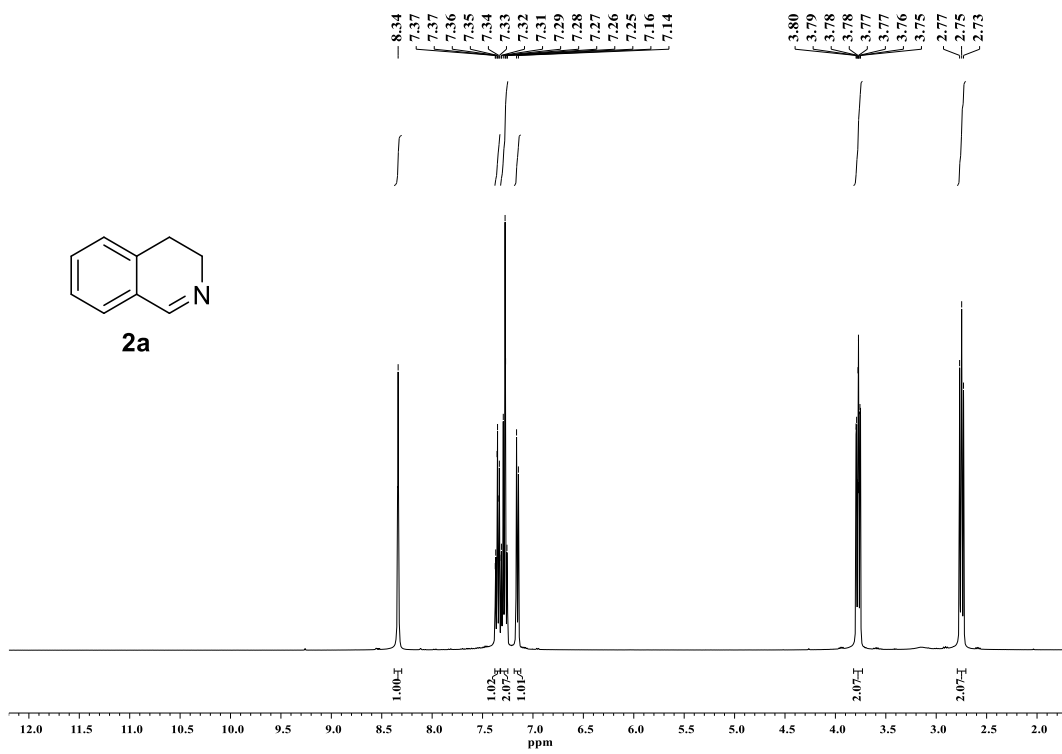
¹H NMR (400 MHz, CDCl₃) δ [ppm] 8.34 (s, 1H), 7.35 (td, *J* = 7.2, 2.0 Hz, 1H), 7.32 – 7.23 (m, 2H), 7.15 (d, *J* = 7.6 Hz, 1H), 3.80 – 3.75 (m, 2H), 2.75 (t, *J* = 8.0 Hz, 2H); **¹³C NMR** (101 MHz, CDCl₃) δ [ppm] 160.43, 136.40, 131.13, 128.57, 127.49, 127.28, 127.15, 47.46, 25.10; **GC-MS** (EI) 131.10, theoretical value for C₉H₉N is 131.17.

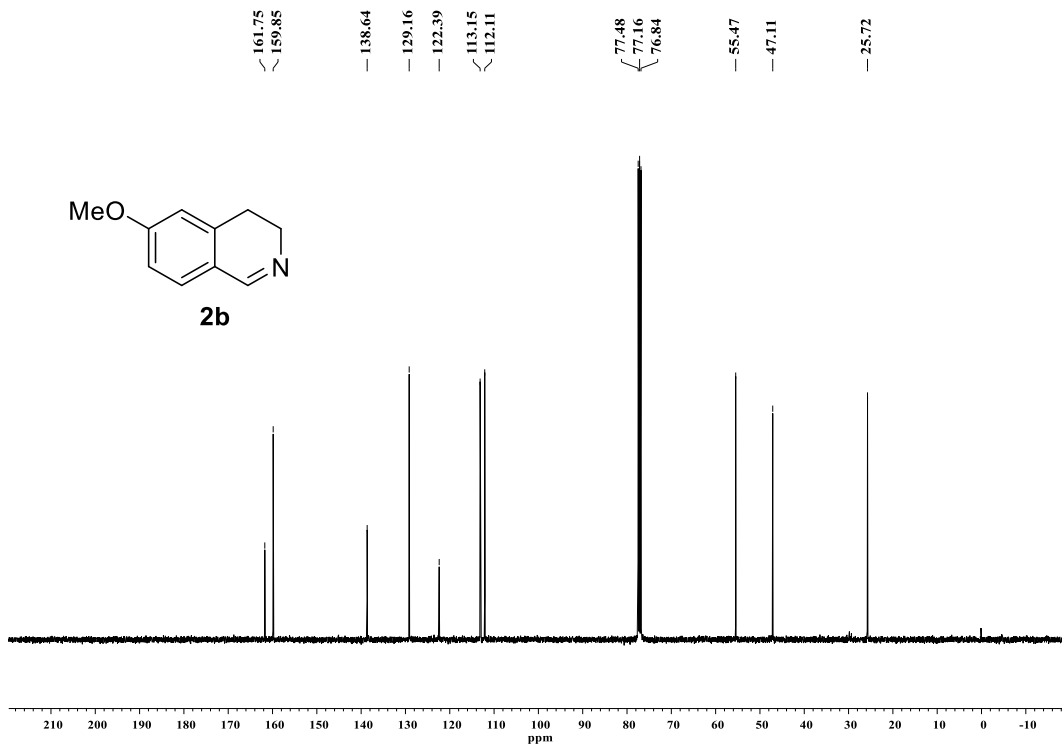
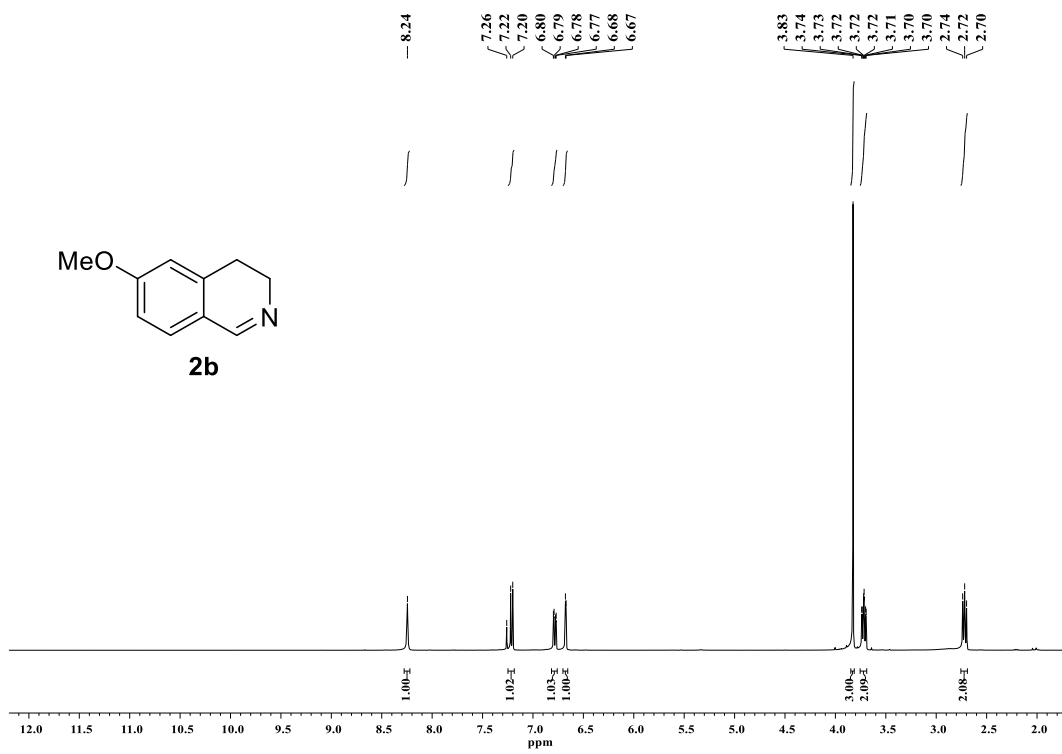


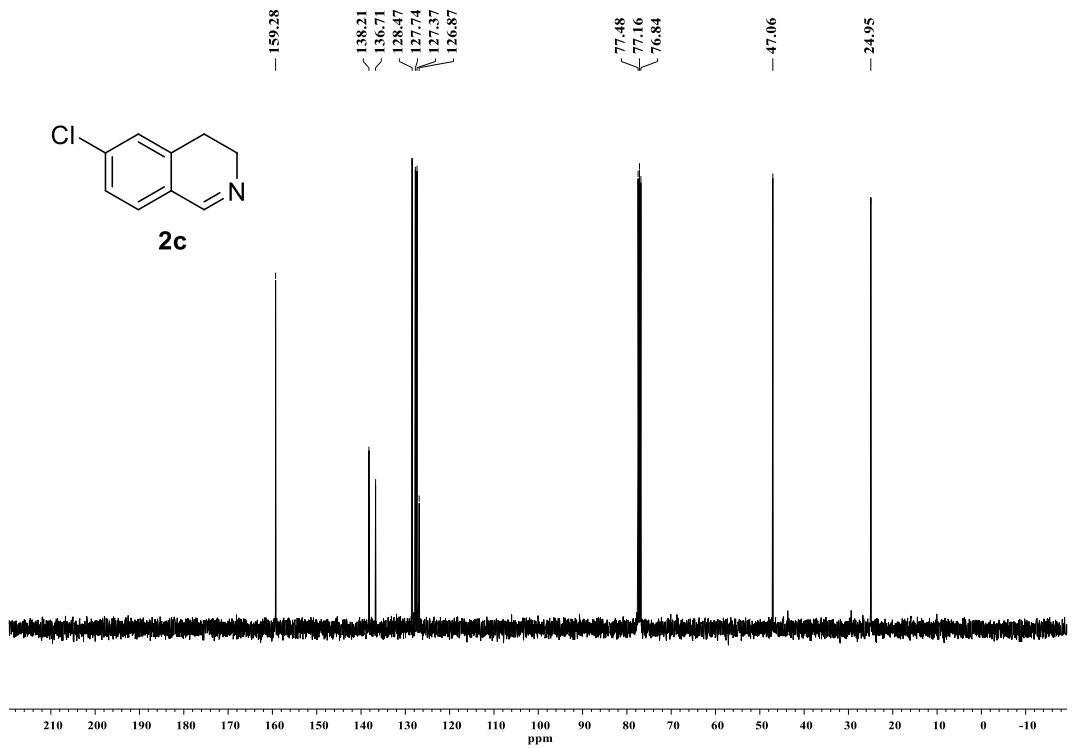
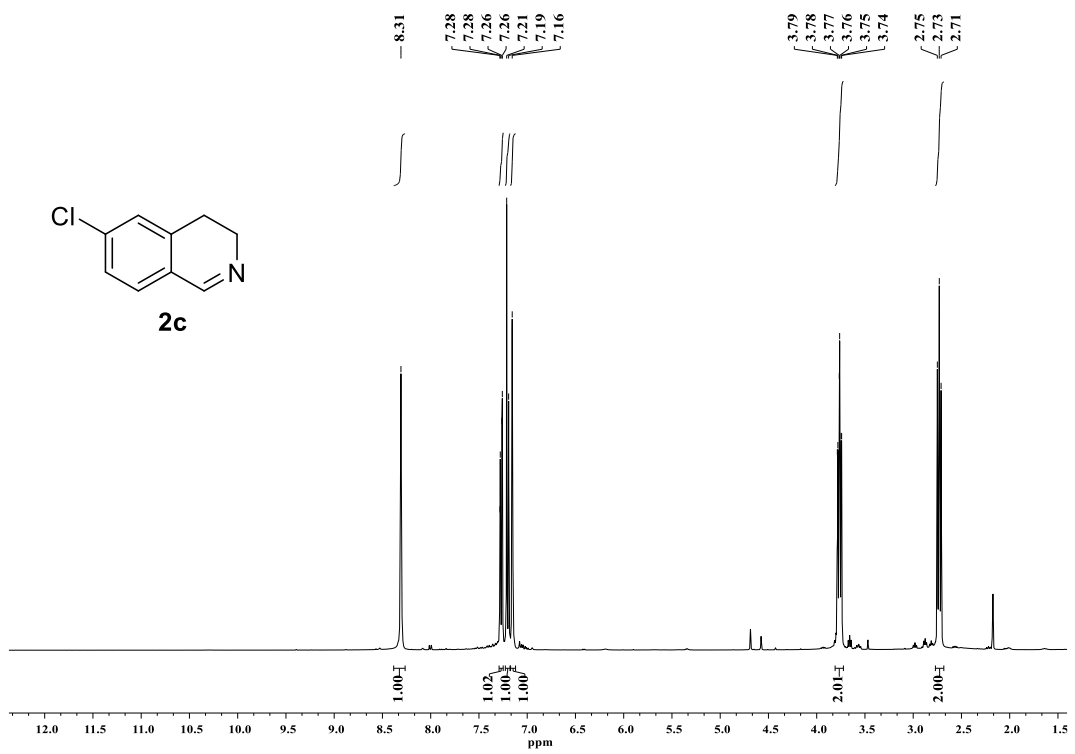
¹H NMR (400 MHz, CDCl₃) δ [ppm] 8.25 (s, 1H), 7.21 (d, *J* = 8.4 Hz, 1H), 6.78 (dd, *J* = 8.4, 2.4 Hz, 1H), 6.68 (d, *J* = 2.4 Hz, 1H), 3.83 (s, 3H), 3.74 – 3.70 (m, 2H), 2.72 (t, *J* = 8.0 Hz, 2H); **¹³C NMR** (101 MHz, CDCl₃) δ [ppm] 161.75, 159.85, 138.64, 129.16, 122.39, 113.15, 112.11, 55.47, 47.11, 25.73; **GC-MS** (EI) 161.09, theoretical value for C₁₀H₁₁NO is 161.22.



¹H NMR (400 MHz, CDCl₃) δ [ppm] 8.31 (s, 1H), 7.27 (dd, *J* = 8.2, 1.6 Hz, 1H), 7.21 – 7.19 (m, 1H), 7.16 (s, 1H), 3.76 (td, *J* = 8.0, 1.6 Hz, 2H), 2.73 (t, *J* = 8.0 Hz, 2H); **¹³C NMR** (101 MHz, CDCl₃) δ [ppm] 159.28, 138.21, 136.71, 128.47, 127.74, 127.37, 126.88, 47.06, 24.95; **GC-MS** (EI) 165.02, theoretical value for C₉H₈ClN is 165.64.







3. References

- (1) Trotochaud, L.; Young, S. L.; Ranney, J. K.; Boettcher, S. W., Nickel-Iron Oxyhydroxide Oxygen-Evolution Electrocatalysts: The Role of Intentional and Incidental Iron Incorporation. *J. Am. Chem. Soc.* **2014**, *136*, 6744-6753.
- (2) Kresse, G.; Furthmüller, J., Efficiency of Ab-Initio Total Energy Calculations for Metals and Semiconductors Using a Plane-Wave Basis Set. *Comp. Mater. Sci.* **1996**, *6*, 15-50.
- (3) Kresse, G.; Furthmüller, J., Efficient Iterative Schemes for Ab Initio Total-Energy Calculations Using a Plane-Wave Basis Set. *Phys. Rev. B* **1996**, *54*, 11169-11186.
- (4) Perdew, J. P.; Burke, K.; Ernzerhof, M., Generalized Gradient Approximation Made Simple. *Phys. Rev. Lett.* **1996**, *77*, 3865-3868.
- (5) Grimme, S., Semiempirical GGA-Type Density Functional Constructed with a Long-Range Dispersion Correction. *J. Comput. Chem* **2006**, *27*, 1787-1799.
- (6) Nørskov, J. K.; Rossmeisl, J.; Logadottir, A.; Lindqvist, L.; Kitchin, J. R.; Bligaard, T.; Jónsson, H., Origin of the Overpotential for Oxygen Reduction at a Fuel-Cell Cathode. *J. Phys. Chem. B* **2004**, *108*, 17886-17892.
- (7) Guo, S.; Heck, K.; Kasiraju, S.; Qian, H.; Zhao, Z.; Grabow, L. C.; Miller, J. T.; Wong, M. S., Insights into Nitrate Reduction over Indium-Decorated Palladium Nanoparticle Catalysts. *ACS Catal.* **2018**, *8*, 503-515.
- (8) Cheng, H.; Cui, P.; Wang, F.; Ding, L. X.; Wang, H., High Efficiency Electrochemical Nitrogen Fixation Achieved with a Lower Pressure Reaction System by Changing the Chemical Equilibrium. *Angew. Chem. Int. Ed.* **2019**, *58*, 15541-15547.
- (9) Liu, X.; Jang, H.; Li, P.; Wang, J.; Qin, Q.; Kim, M. G.; Li, G.; Cho, J., Antimony-Based Composites Loaded on Phosphorus-Doped Carbon for Boosting Faradaic Efficiency of the Electrochemical Nitrogen Reduction Reaction. *Angew. Chem. Int. Ed.* **2019**, *58*, 13329-13334.
- (10) Suryanto, B. H. R.; Wang, D.; Azofra, L. M.; Harb, M.; Cavallo, L.; Jalili, R.; Mitchell, D. R. G.; Chatti, M.; MacFarlane, D. R., MoS₂ Polymorphic Engineering Enhances Selectivity in the Electrochemical Reduction of Nitrogen to Ammonia. *ACS Energy Lett.* **2019**, *4*, 430-435.
- (11) Geng, Z.; Liu, Y.; Kong, X.; Li, P.; Li, K.; Liu, Z.; Du, J.; Shu, M.; Si, R.; Zeng, J., Achieving a Record-High Yield Rate of 120.9 $\mu\text{g}_{\text{NH}_3} \text{mg}^{-1}_{\text{cat.}} \text{h}^{-1}$ for N₂ Electrochemical Reduction over Ru Single-Atom Catalysts. *Adv. Mater.* **2018**, *30*, 1803498.
- (12) Qiu, W.; Xie, X. Y.; Qiu, J.; Fang, W. H.; Liang, R.; Ren, X.; Ji, X.; Cui, G.; Asiri, A. M.; Cui, G.; Tang, B.; Sun, X., High-Performance Artificial Nitrogen Fixation at Ambient Conditions Using a Metal-Free Electrocatalyst. *Nat. Commun.* **2018**, *9*, 3485.
- (13) Hao, Y. C.; Guo, Y.; Chen, L. W.; Shu, M.; Wang, X. Y.; Bu, T. A.; Gao, W. Y.; Zhang, N.; Su, X.; Feng, X.; Zhou, J. W.; Wang, B.; Hu, C. W.; Yin, A. X.; Si, R.; Zhang, Y. W.; Yan, C. H., Promoting Nitrogen Electroreduction to Ammonia with Bismuth Nanocrystals and Potassium Cations in Water. *Nat. Catal.* **2019**, *2*, 448-456.
- (14) Hui, L.; Xue, Y.; Yu, H.; Liu, Y.; Fang, Y.; Xing, C.; Huang, B.; Li, Y., Highly Efficient and Selective Generation of Ammonia and Hydrogen on a Graphdiyne-Based Catalyst. *J. Am. Chem. Soc.* **2019**, *141*, 10677-10683.
- (15) Chen, G. F.; Cao, X.; Wu, S.; Zeng, X.; Ding, L. X.; Zhu, M.; Wang, H., Ammonia Electrosynthesis with High Selectivity under Ambient Conditions via a Li⁺ Incorporation Strategy. *J. Am. Chem. Soc.* **2017**, *139*, 9771-9774.
- (16) Mukherjee, S.; Cullen, D. A.; Karakalos, S.; Liu, K.; Zhang, H.; Zhao, S.; Xu, H.; More, K. L.; Wang, G.; Wu, G., Metal-Organic Framework-Derived Nitrogen-Doped Highly Disordered Carbon for Electrochemical Ammonia Synthesis Using N₂ and H₂O in Alkaline Electrolytes. *Nano Energy* **2018**, *48*, 217-226.

- (17) Wang, R.; Wang, Z.; Xiang, X.; Zhang, R.; Shi, X.; Sun, X., MnO₂ Nanoarrays: An Efficient Catalyst Electrode for Nitrite Electroreduction toward Sensing and NH₃ Synthesis Applications. *Chem. Commun.* **2018**, *54*, 10340-10342.
- (18) Guo, Y.; Stroka, J. R.; Kandemir, B.; Dickerson, C. E.; Bren, K. L., Cobalt Metallopeptide Electrocatalyst for the Selective Reduction of Nitrite to Ammonium. *J. Am. Chem. Soc.* **2018**, *140*, 16888-16892.
- (19) Dreyse, P.; Isaacs, M.; Calfumán, K.; Cáceres, C.; Aliaga, A.; Aguirre, M. J.; Villagra, D., Electrochemical Reduction of Nitrite at Poly-[Ru(5-NO₂-phen)₂Cl] Tetrapyrrolylporphyrin Glassy Carbon Modified Electrode. *Electrochim. Acta* **2011**, *56*, 5230-5237.
- (20) Chebotareva, N.; Nyokong, T., Metallophthalocyanine Catalysed Electroreduction of Nitrate and Nitrite Ions in Alkaline Media. *J. Appl. Electrochem.* **1997**, *27*, 975-981.
- (21) Xu, S.; Kwon, H. Y.; Ashley, D. C.; Chen, C. H.; Jakubikova, E.; Smith, J. M., Intramolecular Hydrogen Bonding Facilitates Electrocatalytic Reduction of Nitrite in Aqueous Solutions. *Inorg. Chem.* **2019**, *58*, 9443-9451.
- (22) He, D.; Li, Y.; Ooka, H.; Go, Y. K.; Jin, F.; Kim, S. H.; Nakamura, R., Selective Electrocatalytic Reduction of Nitrite to Dinitrogen Based on Decoupled Proton-Electron Transfer. *J. Am. Chem. Soc.* **2018**, *140*, 2012-2015.
- (23) Duca, M.; Khamseh, S.; Lai, S. C. S.; Koper, M. T. M., The Influence of Solution-Phase HNO₂ Decomposition on the Electrocatalytic Nitrite Reduction at a Hemin-Pyrolitic Graphite Electrode. *Langmuir* **2010**, *26*, 12418-12424.